

Hepatic glycerol shunt and glycerol-3-phosphate phosphatase control liver metabolism and glucodetoxification under hyperglycemia



Anfal Al-Mass^{1,2}, Pegah Poursharifi², Marie-Line Peyot², Roxane Lussier², Isabelle Chenier², Yat Hei Leung², Anindya Ghosh², Abel Oppong², Elite Possik², Yves Mugabo², Rasheed Ahmad³, Robert Sladek¹, S.R. Murthy Madiraju^{2,***}, Fahd Al-Mulla³, Marc Prentki^{2,*}

ABSTRACT

Objective: Glycerol-3-phosphate (Gro3P) phosphatase (G3PP) hydrolyzes Gro3P to glycerol that exits the cell, thereby operating a “glycerol shunt”, a metabolic pathway that we identified recently in mammalian cells. We have investigated the role of G3PP and the glycerol shunt in the regulation of glucose metabolism and lipogenesis in mouse liver.

Methods: We generated hepatocyte-specific G3PP-KO mice (LKO), by injecting AAV8-TBG-*iCre* to male G3PP^{fl/fl} mice. Controls received AAV8-TBG-*eGFP*. Both groups were fed chow diet for 10 weeks. Hyperglycemia (16–20 mM) was induced by glucose infusion for 55 h. Hepatocytes were isolated from normoglycemic mice for *ex vivo* studies and targeted metabolomics were measured in mice liver after glucose infusion.

Results: LKO mice showed no change in body weight, food intake, fed and fasted glycemia but had increased fed plasma triglycerides. Hepatic glucose production from glycerol was increased in fasted LKO mice. LKO mouse hepatocytes displayed reduced glycerol production, elevated triglyceride and lactate production at high glucose concentration. Hyperglycemia in LKO mice led to increased liver weight and accumulation of triglycerides, glycogen and cholesterol together with elevated levels of Gro3P, dihydroxyacetone phosphate, acetyl-CoA and some Krebs cycle intermediates in liver. Hyperglycemic LKO mouse liver showed elevated expression of proinflammatory cytokines and M1-macrophage markers accompanied by increased plasma triglycerides, LDL/VLDL, urea and uric acid and myocardial triglycerides.

Conclusions: The glycerol shunt orchestrated by G3PP acts as a glucose excess detoxification pathway in hepatocytes by preventing metabolic disturbances that contribute to enhanced liver fat, glycogen storage, inflammation and lipid build-up in the heart. We propose G3PP as a novel therapeutic target for hepatic disorders linked to nutrient excess.

© 2022 The Authors. Published by Elsevier GmbH. This is an open access article under the CC BY-NC-ND license (<http://creativecommons.org/licenses/by-nc-nd/4.0/>).

Keywords Glycerol-3-phosphate phosphatase; Glycerol shunt; Glucodetoxification; Liver; Lipogenesis; Triglycerides; Cholesterol; Glycogen; Inflammation; NAFLD

1. INTRODUCTION

Chronic nutritional excess results in metabolic disorders such as obesity, type 2 diabetes (T2D), ectopic accumulation of triglycerides (TG) and non-alcoholic fatty liver disease (NAFLD). Prolonged fuel surfeit causes hyperinsulinemia, fat build-up and metabolic stress in various organs, leading to insulin resistance, β -cell failure and T2D [1–4]. Central to these metabolic diseases are disturbances in glucose, lipid and energy metabolism in association with deranged insulin homeostasis and inflammation [1,2,5]. The pathogenesis of NAFLD starts with the disturbed lipid metabolism in liver, accumulation of TG and enhanced inflammation, which progressively lead to fibrosis,

non-alcoholic steatohepatitis (NASH), cirrhosis and hepatocellular carcinoma [6–10]. Several studies from our lab [1,5,11–14] and elsewhere [15,16] highlighted the significance of the glycerolipid/free fatty acid (GL/FFA) cycle in T2D, obesity and pancreatic β -cell function. The GL/FFA cycle with its lipogenesis and lipolysis arms, connects lipid and glucose metabolism via glucose-derived glycerol-3-phosphate (Gro3P) and FFA-derived fatty acyl-CoA, the substrates for lipogenesis [11,17]. Chronic nutrient surfeit promotes the accumulation of TG in liver by augmenting the lipogenic segment of the GL/FFA cycle by providing Gro3P and FFA [1,11,13].

Glucose-derived Gro3P links glucose, lipid and energy metabolism in all cells, as it is produced during glycolysis, serves as a substrate for

¹Department of Medicine, McGill University, Montréal, QC, Canada ²Departments of Nutrition, Biochemistry and Molecular Medicine, University of Montreal, and Montreal Diabetes Research Center and CRCHUM, Montréal, QC, Canada ³Departments of Immunology, Microbiology, Genetics and Bioinformatics, Dasman Diabetes Institute, Dasman 15462, Kuwait

*Corresponding author. Biochemistry and Molecular Medicine, Université de Montréal CRCHUM, Room R08-412, Tour Viger, 900 rue Saint Denis Montreal, QC H2X 0A9, Canada. E-mail: marc.prentki@umontreal.ca (M. Prentki).

**Corresponding author. CRCHUM, Room R08-418, Tour Viger, 900 rue Saint Denis, Montreal, QC H2X 0A9, Canada. E-mail: s.r.murthy.madiraju.chum@ssss.gouv.qc.ca (S.R. Murthy Madiraju).

Received September 26, 2022 • Accepted September 30, 2022 • Available online 2 October 2022

<https://doi.org/10.1016/j.molmet.2022.101609>

glycerolipid synthesis and participates in the electron shuttle between cytosol and mitochondria [18,19]. We earlier discovered a novel mammalian metabolic enzyme, lying at the heart of intermediary metabolism, Gro3P phosphatase (G3PP), and demonstrated that G3PP directly converts part of the excess glucose-derived Gro3P to less toxic glycerol, which leaves the cell [18]. We named this novel metabolic pathway the *glycerol shunt* that possibly helps in glucodetoxification in pancreatic β -cells [20] and demonstrated that G3PP-glycerol shunt pathway confers better healthspan and lifespan in *C. elegans* [21]. Hydrolytic control of intracellular Gro3P by G3PP adds another layer of metabolic regulation that was not recognized previously in mammalian cells. G3PP was initially identified as phosphoglycolate phosphatase with its gene name as *PGP*, but we and others showed that its actual primary physiological function involves Gro3P hydrolysis, although it can hydrolyze some other phospho-metabolites produced in particular during cellular stress [18,20,22–24]. Our earlier *in vitro* studies support a role for G3PP in liver glucose and lipid metabolism and showed an inverse relationship between G3PP expression and lipogenesis in isolated rat hepatocytes [18] and that the impact of G3PP activity on metabolism is more evident at high glucose concentrations when intracellular Gro3P rises to sufficiently high levels to become available for G3PP [18]. Despite the significant evidence for G3PP mediated regulation of metabolism in hepatocytes *in vitro*, the role of this enzyme *in vivo* in liver is not known. We earlier observed that supra-physiological overexpression (more than 50 fold) of G3PP in rat liver *in vivo*, led to decreased gluconeogenesis from glycerol and plasma TG and elevated plasma glycerol [18]. Though these limited studies were compatible with an *in vivo* function of G3PP in Gro3P hydrolysis, the pathophysiological significance of G3PP in liver remains to be discovered. Our recent studies demonstrated that β -cell specific G3PP deletion in normal diet fed mice enhances glucose stimulated insulin secretion, promotes glucose oxidation and lipogenesis in the islets, and renders the islets susceptible to glucotoxicity in terms of excess insulin secretion and apoptosis and these changes are associated with elevated islet Gro3P levels [20]. Considering that G3PP is well expressed in the liver [18] and that this tissue plays central role in energy metabolism and metabolic disorders associated with fuel excess, the present studies were conducted to address the precise *in vivo* role of G3PP in liver glucose and fat metabolism and test the view that the glycerol shunt is implicated in hepatic glucodetoxification.

2. MATERIALS AND METHODS

2.1. Animals

G3PP^{lox/lox} mice in which exons 1 and 2 of *PGP* (coding for G3PP protein) gene are flanked with LoxP sites were generated by Ingenious Targeting Laboratory (Stony Brook, NY). At 8 weeks of age, male G3PP^{lox/lox} (*fl/fl*) mice received a single tail vein injection of 5×10^{10} genome copies (GC)/mouse of AAV8-TBG-*iCre* (Vector Biolabs: VB1724) or AAV8-TBG-*eGFP* (Vector Biolabs: VB1743) or saline (Figure 1A). The TBG (Thyroxine Binding Globulin) promoter drives hepatocyte-specific gene expression [25]. Mice were placed in individual cages and fed a normal chow diet (15% fat by energy; Envigo RMS (Canada) limited. T2918) ad libitum for 10 weeks. Body weight and food intake were measured weekly. At beginning of week 10, fed glycemia was measured at 8:00 AM and then the mice were fasted overnight for 16 h and fasted glycemia was measured next day at 8:00 AM. Then all the mice were re-fed and were sacrificed at the end of the week for tissue and blood collection. All procedures were approved by the Institutional committee for the protection of animals (Comité Institutionnel de Protection des Animaux du Centre Hospitalier de l'Université de Montréal).

2.2. Western blot analysis for the validation of hepatocyte specific G3PP deletion

After 4 weeks following AAV8 viral infection, mice were anesthetized and the livers were perfused with collagenase buffer for hepatocyte preparation (see below for details) and visceral adipose tissue, brain and skeletal muscle were collected. Mouse tissues and isolated hepatocytes were lysed in RIPA buffer (10 mM Tris-HCl, 1 mM EDTA, 0.5 mM EGTA, 1% Triton X-100, 0.1% sodium deoxycholate, 0.1% sodium dodecylsulfate and 140 mM NaCl) and the protein extracts were used for western blot analysis to validate hepatocyte-specific G3PP deletion (G3PP primary antibody: PGP Antibody (E-10) (sc-390 883), secondary antibody: m-IgG κ BP-HRP (sc-516 102) both from Santa Cruz Biotechnology). For all tissues, α -tubulin was used as the gel loading control.

2.3. Oral glycerol load test

Mice were fasted for 16 h, after 4 weeks following AAV8 infection, and were administered glycerol at 5 mg/g BW (using 87% wt/vol, glycerol in water) by gavage. Blood was collected from tail vein at baseline and at 5, 10, 15, 20, 30, 45 and 60 min following the glycerol load and blood glucose was measured using a glucometer.

2.4. Pyruvate load test

After completing the glycerol load test at 4 weeks following AAV8 infection, mice were rested for 2 weeks. At 6 weeks after AAV8 infection, mice were fasted for 16 h and sodium pyruvate (at 1 mg/g BW, in water) was injected intraperitoneally. Blood was collected from the tail vein at baseline and 5, 10, 15, 20, 30, 45, and 60 min following the pyruvate load and blood glucose was measured using a glucometer.

2.5. Hepatocyte isolation

Hepatocytes were isolated from mice 4 weeks after AAV8 infection, by *in situ* collagenase (type XI; Sigma) perfusion [18] and were seeded in DMEM complete media (Sigma D5030) (pH 7.4) without phenol red, supplemented with 0.48 mM of sodium bicarbonate, 5 mM glucose, 1 mM sodium pyruvate, 2 mM glutamine, penicillin streptomycin, 0.2% BSA, 1 nM insulin and 100 nM dexamethasone) using Collagen I Coated Plate (A11428-01) [18]. *Ex-vivo* experiments were done after 16 h following seeding.

2.6. Gluconeogenesis in hepatocytes, *ex vivo*

Primary mouse hepatocytes, attached to the collagen plates for 16 h following seeding, were washed twice with PBS and starved in DMEM without glucose for 3 h. Then the cells were washed with PBS, followed by incubation for 3 h in glucose production medium (pH 7.4) consisting of glucose-free DMEM without phenol red, supplemented with 15 mM Hepes and 2 mM L-glutamine, and 10 mM glycerol or 20 mM sodium lactate plus 2 mM sodium pyruvate. After incubation, the medium was collected for glucose measurement (Autokit Glucose; Wako) and the hepatocytes were collected for protein measurement [18].

2.7. Triglyceride, glycerol and lactate production in hepatocytes, *ex vivo*

Primary mouse hepatocytes, attached to the collagen plates, were washed with PBS and incubated in DMEM complete media containing 5 or 25 mM glucose for 2 h. After incubations, media and cells were collected to measure glycerol and lactate release and TG and lactate content, respectively, as described before [18].

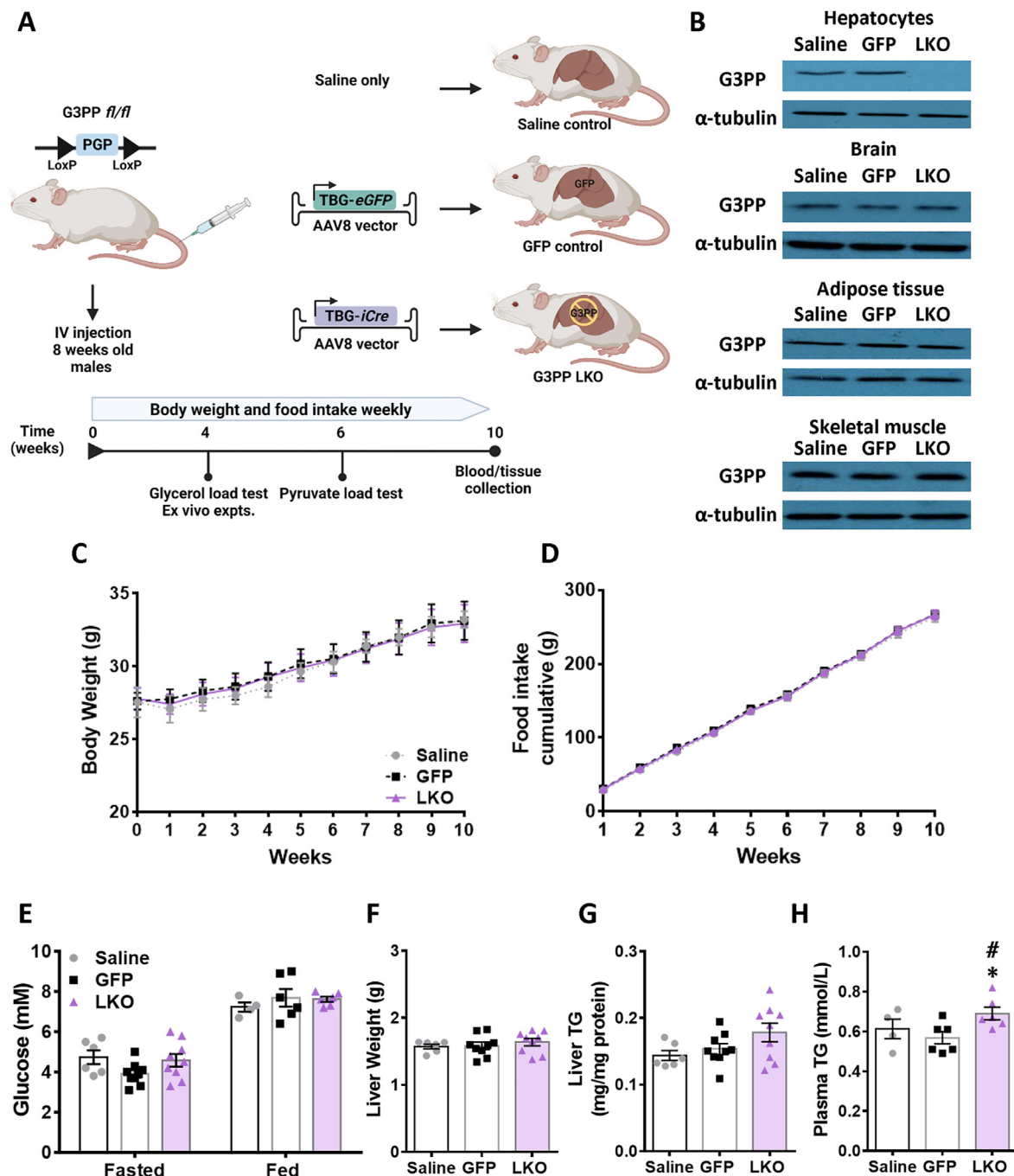


Figure 1: Generation and phenotyping of hepatocyte specific G3PP-KO (LKO) mice. (A) Schematic protocol for creating the LKO and control mice and the experimental design in this study. Male, 8 wk old G3PP^{f/f} mice were injected with AAV8-TBG-Cre or AAV8-TBG-eGFP viral vectors or saline vehicle through the tail vein. Mice were then kept on chow diet for 10 weeks and sacrificed at indicated time and blood and tissues were collected for analyses. (B) Validation of G3PP deletion by Western blot using protein extracts from hepatocytes, brain, adipose tissue and skeletal muscle from mice, 4 weeks after IV injections (saline, n = 3; GFP, n = 3; LKO, n = 4); α -tubulin was used as a control of protein loading. (C) Body weight, (D) food intake, (E) fed and fasted glycemia, (F) liver weight, (G) liver TG content (H) Fed plasma triglycerides. N = 6–9 per group as shown; means \pm SEM; *p < 0.05 vs GFP control, #p < 0.05 vs saline control. Two-way ANOVA was used to analyze results in panels C & D, and one-way ANOVA was used for analysis of results in panels E to H.

2.8. In vivo glucose infusion

After 4 weeks following infection of the G3PP^{lox/lox} mice with AAV8-TBG-Cre (LKO) or AAV8-TBG-eGFP (control), a cannula was inserted in the right jugular vein (Figure 3A). The mice were subcutaneously injected with carprofen (20 mg/kg) combined with saline (around 3 ml) to reduce pain, prior to surgery and were anesthetised with isoflurane.

Cages were placed on a heating pad with a cold spot (1/3 cold). Diet gel (DietGel 31 M: 72-08-5022) was given to the mice during the post-operation period with pellets in the bottom of the cages for the entire time. In the post-operation period, mice were infused with 5U heparinized saline (7 μ l/h) to make sure that the cannula remained unclogged. The mice were given a second injection of carprofen

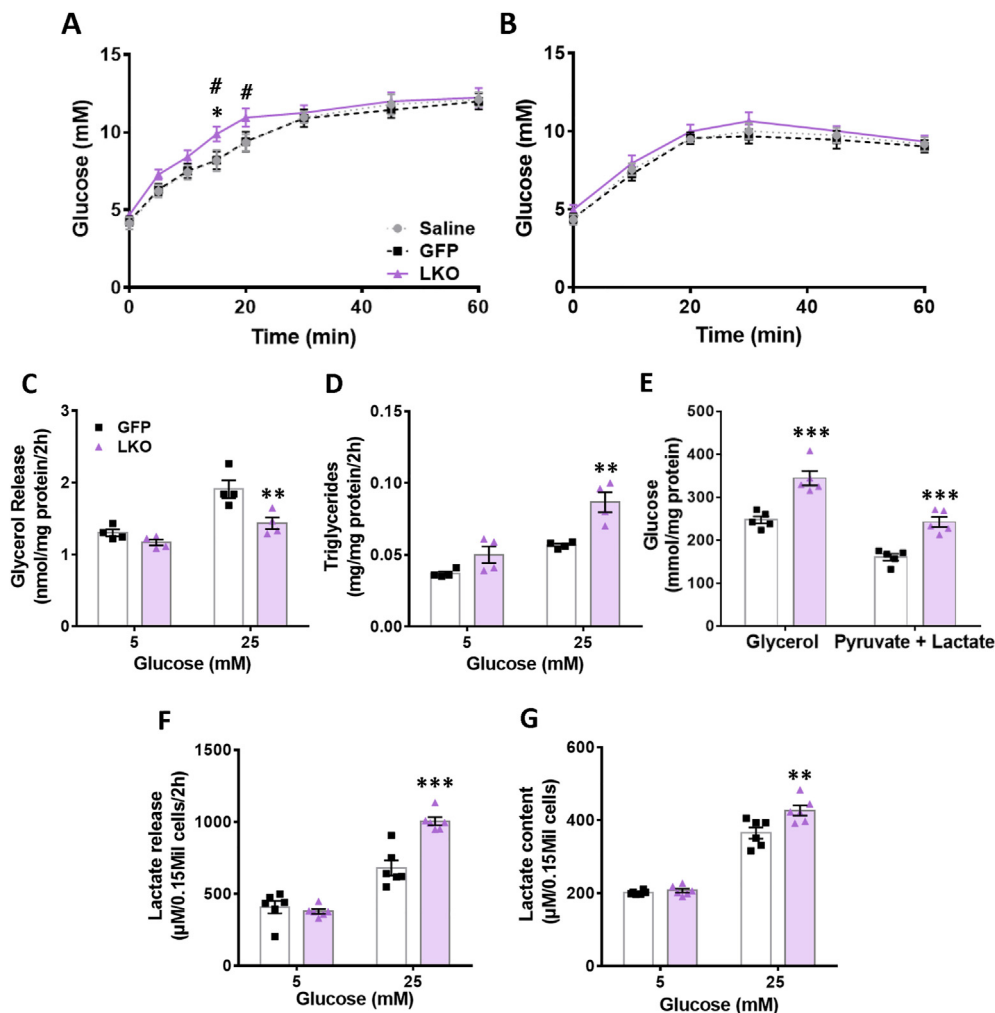


Figure 2: Isolated LKO hepatocytes show decreased glycerol release and increased TG content, glycolytic flux and gluconeogenesis. Glycerol (5 mg/g BW, i. p.) and pyruvate (1 mg/g BW, i. p.) were administered to 16 h fasted LKO and control mice, and tail blood glycemia was measured. (A) Glycerol and (B) pyruvate load tests (saline, n = 6; GFP, n = 9; LKO, n = 9). Means ± SEM; *p < 0.05 LKO vs both controls, with two-way ANOVA for 0–60 min; #p < 0.05 LKO vs GFP-control, with two-way ANOVA for 0–20 min. Hepatocytes were isolated from LKO and control mice and incubated at 5 and 25 mM glucose, for measuring glycerol release, TG content and lactate content and release. For measuring gluconeogenesis, hepatocytes were glucose starved and incubated with 10 mM glycerol or 20 mM lactate plus 2 mM pyruvate. (C) glycerol release, (D) triglyceride content, (E) gluconeogenesis from glycerol or pyruvate/lactate, (F) lactate release, (G) lactate content. n = 4–6 per group as shown. *p < 0.05, **p < 0.01, and ***p < 0.001 vs. GFP control and #p < 0.05 vs saline control; Two-way ANOVA.

(20 mg/kg) and 3 ml of saline on the first post-operative day. Following surgery, fresh diet gel was given daily and the mice were also given saline daily based on their hydration status, evaluated by their appearance and attitude in the cage [26]. Five days following surgery, the mice were infused with dextrose 70%. The glucose infusion rate (GIR) started at 30 mg/kg/min and was adjusted every 3 h during the day and once during the night to maintain the blood glucose at pre-determined level (14–16 mM). Glycemia was measured in the tail blood using a glucometer (Contour blood glucometer, Bayer). During the glucose infusion, blood and urine [27] were collected twice daily. The glucose infusion was continued for 55 h and then the mice were euthanized using ketamine/xylazine and blood, liver and heart were collected at necropsy.

2.9. Liver analytes

Livers from normal diet (10 weeks) and glucose-infused mice were collected and snap-frozen in liquid nitrogen. TG was measured after

lipid extraction [18] using a triglyceride reagent (Sigma–Aldrich cat: T2449). For glucose-infused mice, liver glycogen and total cholesterol were determined by colorimetric assays (Abcam Glycogen Assay Kit, ab65620; and Abcam Cholesterol Assay Kit, ab65390).

2.10. Plasma analytes

Lipid profile (Cobas kits used: cholesterol, ref: 04718917 190; triglycerides (TGs), ref: 04657594 190; high density lipoproteins (HDL), ref: 07528604 190; low density lipoproteins (LDL), ref: 07005806 190) and liver function markers (Cobas kits used: alanine aminotransferase (ALT), ref: 04718569 190; alkaline phosphatase (ALP), ref: 04657373 190; albumin, ref: 04657357 190; aspartate aminotransferase (AST), ref: 04657543 190; urea, ref: 04657616 190; uric acid, ref: 04657608 190) were measured in the plasma from normal diet (10 weeks) and/or glucose-infused mice using a Cobas C111 analyzer (Roche, Switzerland) [28]. Plasma samples from glucose-infused mice were also measured for the following: insulin (insulin: AL204, Perkin

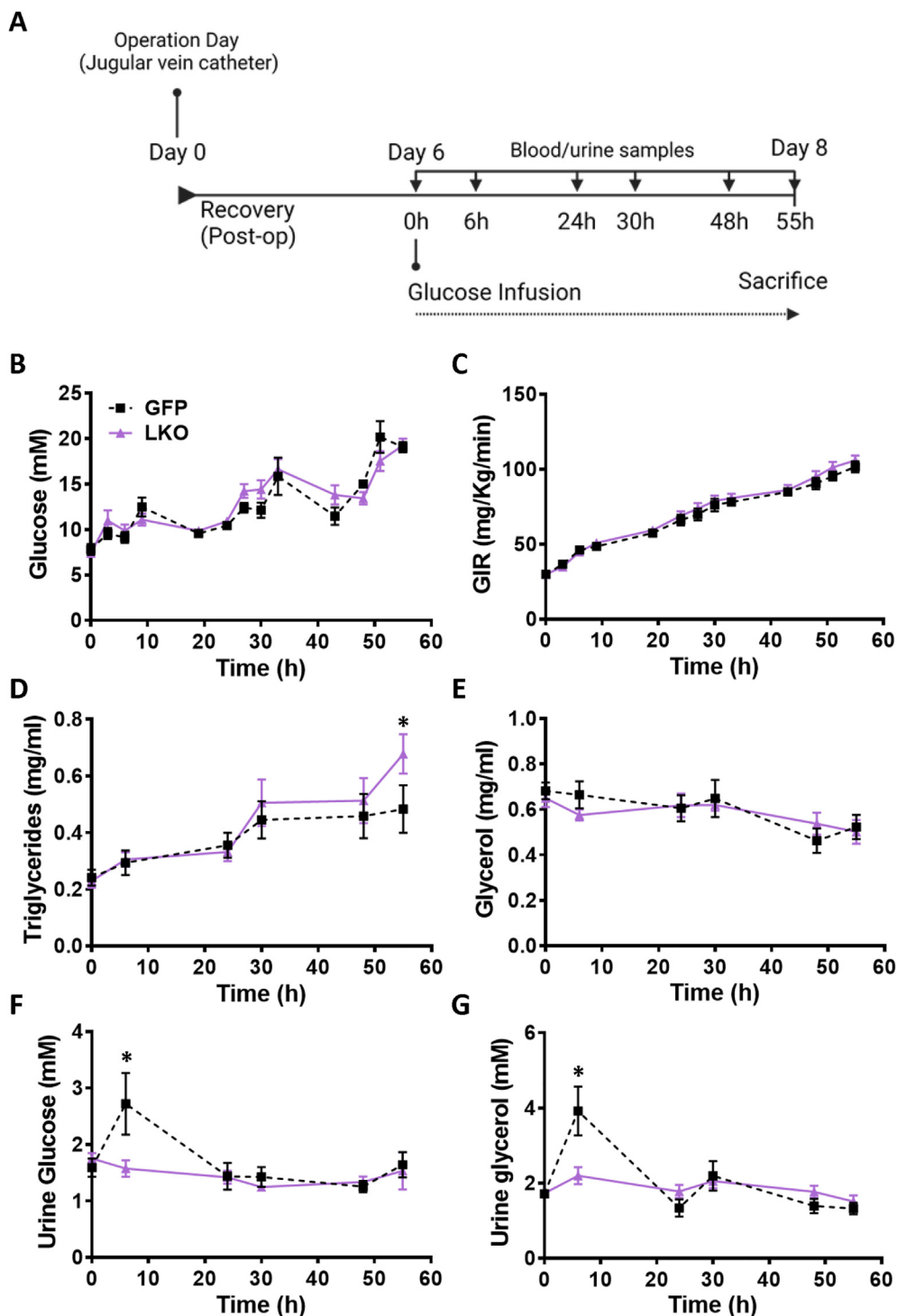


Figure 3: *In vivo* glucose infusion causes increased plasma TG and reduced urine glycerol in LKO mice. (A) Timeline of glucose infusion experiment. Mice were inserted with a catheter in the jugular vein and a continuous intravenous 55 h infusion of glucose was maintained. Arterial blood and urine were collected twice a day. (B) Blood glucose and (C) glucose infusion rate (GIR) were monitored and the infusion rate was adjusted to maintain hyperglycemia. (D) Plasma TG. (E) Plasma glycerol. (F) Glucose in urine. (G) Glycerol in urine. Means \pm SEM; GFP-control, n = 6; LKO, n = 8; *p < 0.05 vs GFP control; Two-way ANOVA.

Elmer); LDL/VLDL (Cholesterol Assay Kit - HDL and LDL/VLDL (ab65390)); and inflammation markers (IL-6: AL504, Perkin Elmer, TNF α : AL505, Perkin Elmer and CRP: ab157712, ABCAM). Plasma LDL/VLDL, insulin and inflammation markers were measured using EnVision from Perkin Elmer at the Metabolomic Core Facility of CRCHUM.

2.11. RNA extraction and quantitative PCR

Total RNA was extracted from the livers of glucose-infused mice (RNeasy Micro Kit, Qiagen). Following reverse-transcription to cDNA, expression of various genes was determined by quantitative PCR using SYBR Green (Qiagen QuantiTect). All gene expression analyses were

conducted in duplicate and normalized to the expression of *18S*. PCR primer sequences are listed in [Supplementary Table 1](#).

2.12. Targeted metabolomics

For metabolomics studies we used a separate cohort of mice that were euthanized by cervical dislocation at the end of glucose infusion and the livers were collected within 45 s and snap-frozen in liquid nitrogen. Then the livers were stored at -80°C . All metabolites described in this study were extracted and measured using an LC-electrospray ionization-MS/MS system (Agilent 1200 SL and a triple-quadrupole mass spectrometer (4000Q TRAP MS/MS, Sciex) as described before [18,29]. Peak areas were used for relative quantification of the identified metabolites. All these analyses were done at the CRCHUM Metabolomic Core Facility.

2.13. Statistical analyses

Data were analyzed using GraphPad Prism 6 (GraphPad Software, San Diego, CA). Results are expressed as means \pm SEM. Differences between two groups were assessed by unpaired, two-tailed Student's *t* test, and between multiple groups using one-way or two-way analyses of variance (ANOVA) with Bonferroni correction, as indicated. A *p* value < 0.05 , following correction for multiple testing as appropriate, was considered statistically significant.

3. RESULTS

3.1. Phenotypic characterization of G3PP-LKO mice on chow diet

G3PP protein levels were markedly decreased in LKO hepatocytes compared to controls (G3PP *fl/fl* mice injected with AAV8-TBG-GFP viral vector or saline vehicle) without any change in G3PP expression in extrahepatic tissues (brain, adipose, kidney, heart and muscles) obtained from LKO mice four weeks following AAV8 infection (Figure 1B). G3PP-LKO mice fed chow diet for 10 weeks following AAV8-TBG-*iCre* injection, showed no change in body weight gain or food intake (Figure 1C and 1D) and no differences in fed and fasted glycemia compared to the two control mice (Figure 1E). At the end of the study, LKO mice showed no change in the weights of liver (Figure 1F) or other tissues (Figure S1A) compared to control animals. There were also no differences in the plasma levels of liver function markers (such as alanine aminotransferase, ALT; alkaline phosphatase, ALP; and albumin), total cholesterol, high density lipoprotein (HDL) and low density lipoprotein (LDL) between LKO and control mice (Figure S1B). However, the LKO mice showed significantly elevated plasma TG but with only a slight increase in liver TG content ($p=0.7$), compared to the control mice (Figure 1G, 1H).

3.2. Increased glucose production following a glycerol load in LKO mice

In order to assess if deletion of G3PP in hepatocytes affects gluconeogenesis *in vivo*, we conducted glycerol and pyruvate load test after 16 h fasting to deplete glycogen stores. A small but significant increase in plasma glucose levels was observed following a glycerol oral load in the LKO mice compared to controls, likely due to elevated hepatic glucose production (Figure 2A). However, LKO mice did not show a change in glucose production following a pyruvate load (Figure 2B).

3.3. LKO hepatocytes show *ex vivo* decreased glycerol release and increased TG content, glycolytic flux and gluconeogenesis

As there was no difference between the many *in vivo* and *ex vivo* parameters measured above in saline-treated and GFP-control mice, we focused on GFP group as the main control as this group of mice

received the same dose of AAV8 viral particles as the LKO mice. Isolated LKO hepatocytes showed significantly decreased glycerol release (Figure 2C) and increased TG content (Figure 2D) compared to control hepatocytes when incubated at high glucose (25 mM) but not at basal glucose (5 mM) concentration. *Ex vivo* gluconeogenesis in the LKO hepatocytes was found to be elevated with glycerol as a substrate compared to controls (Figure 2E) and this increase was also seen using pyruvate/lactate as substrates (Figure 2E), though this was not seen *in vivo* (Figure 2B). Furthermore, LKO hepatocytes showed significantly elevated lactate release (Figure 2F) and content (Figure 2G) only at high glucose concentration. These findings indicate an elevated glycolytic flux at high glucose concentrations in the LKO hepatocytes. These *ex vivo* results with LKO mouse hepatocytes are consistent with our previous *in vitro* findings in rat hepatocytes with RNAi-knockdown of G3PP [18] and validate the present LKO mouse model.

3.4. G3PP LKO mice show a transient reduction in urinary glycerol, liver lipid and glycogen accumulation, and increased plasma lipids, lipoproteins and urate during provoked chronic hyperglycemia

Results from LKO hepatocytes, *ex vivo*, suggested that G3PP activity in hepatocytes has more impact on metabolism at high glucose concentrations. In order to assess *in vivo* the influence of elevated glucose supply on liver metabolism in LKO mice, we infused the LKO and control mice with a glucose solution to elevate glycemia above the physiological levels, between 16 mM and 20 mM, for a period of 55 h (Figure 3A). There was no difference in the body weight between the LKO and control mice at baseline (after implantation of an indwelling canula, 5 days before glucose infusion) and at the start and end of glucose infusion (Figure S2A). Glycemia and glucose infusion rate (GIR) during the infusion were similar in both LKO and control mice (Figure 3B–3C). We have chosen a prolonged period of glucose infusion to assess the ability of liver to handle excess glucose when supplied for relatively longer duration—mimicking glucotoxic conditions as may occur under uncontrolled diabetes. Under these experimental conditions we examined if the presence or absence of G3PP and the glycerol shunt makes a difference in the hepatocytes' ability to metabolize and manage excess glucose levels. While it is possible that 55 h of hyperglycemia at 16–20 mM may cause some glucose intolerance, its extent would be the same in both GFP-control and LKO mice, as the plasma insulin values were the same in these groups of mice (see Figure S2B). In addition, the GIR was the same in both groups (Figure 3C), again suggesting that any whole body glucose homeostatic disturbances during the glucose infusion are similar in both groups. Average blood glucose levels were 10–11 mM during the first 24 h of the infusion; 13–15 mM from 24 h to 48 h; and 18–19 mM from 48 h to 55 h of infusion for both the groups of mice. Plasma TG during glucose infusion increased with time in both groups, with LKO mice showing a significant increase at the end of the infusion compared to the control mice (Figure 3D). Plasma glycerol was not different during glucose infusion between the two groups (Figure 3E). Urinary glucose and glycerol at 6 h post the start of glucose infusions were both elevated by about twofold in the control mice. but this rise in both metabolites did not occur in the LKO mice. However at subsequent times all glucose and glycerol levels in urine returned to basal values and were not different in LKO vs control mice (Figure 3F–3G). At the end of the 55 h glucose infusion, liver weight (Figure 4A) and liver TG (Figure 4B), glycogen (Figure 4C) and total and free cholesterol (Figure 4D) in LKO mice were significantly elevated compared to the control mice. In addition, heart TG levels were also found to be increased in the LKO mice (Figure 4E). Furthermore, following glucose infusion, plasma levels of TG (Figure 4F), LDL + VLDL (Figure 4H), urea

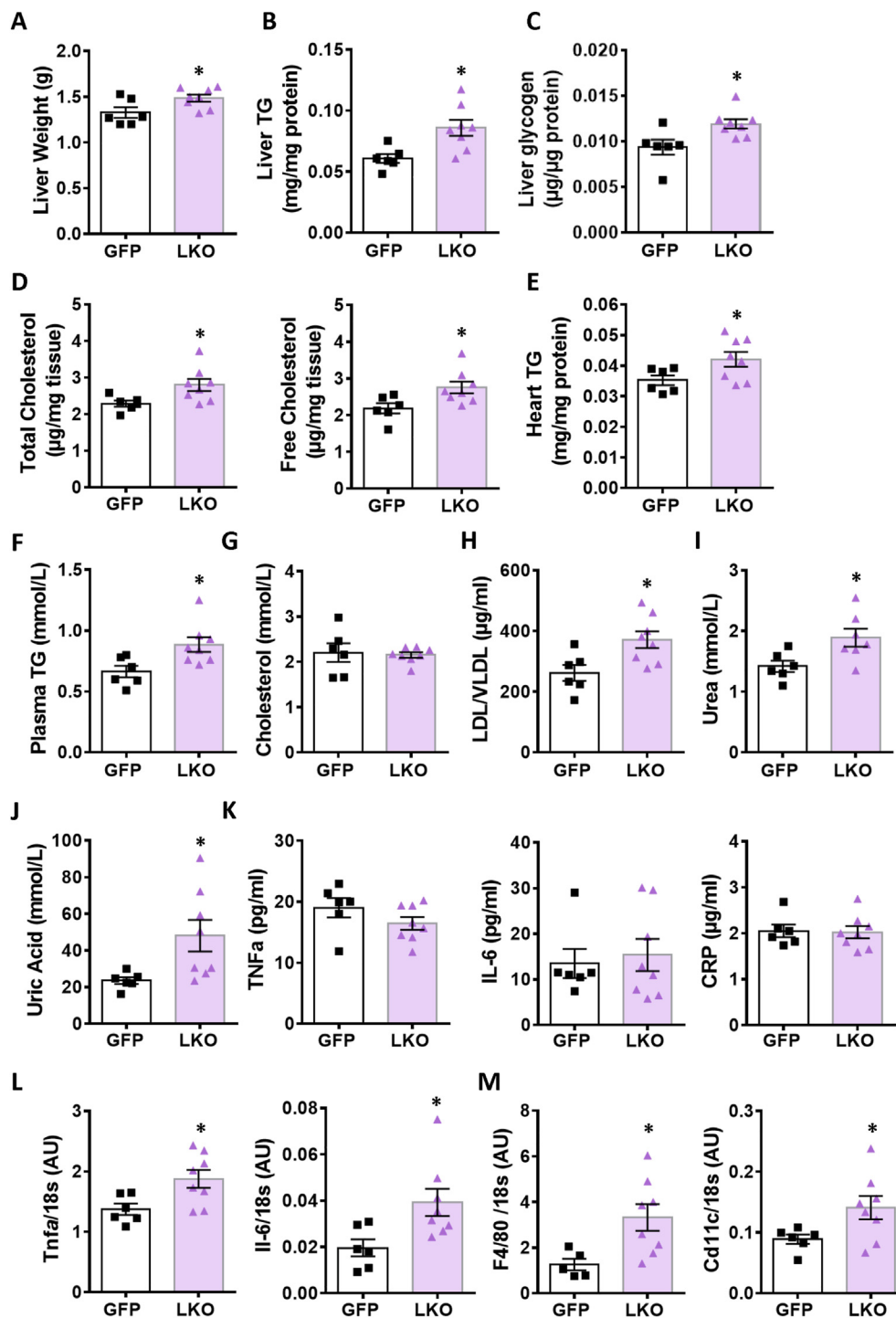


Figure 4: Liver and plasma analytes and inflammation-related liver gene expression in LKO and control mice under hyperglycemia. (A) Liver weight, (B) TG content, (C) glycogen content, (D) total and free cholesterol. (E) Heart TG content. (F) Plasma TG, (G) cholesterol, (H) LDL/VLDL, (I) urea, (J) and uric acid. (K) Plasma inflammation markers: TNF α , IL-6 and C-reactive protein (CRP). (L) Liver cytokines mRNA expression of *Tnfa* and *Il-6*. (M) Liver mRNA markers of macrophages *F4/80* and *Cd11c*. Means \pm SEM (GFP-Control, n = 6; LKO, n = 8). *p < 0.05 vs GFP control; Student's *t* test.

(Figure 4) and uric acid (Figure 4J) were significantly elevated in the LKO mice, but no changes were seen in total cholesterol (Figure 4G) and HDL levels (Figure S2C) compared with control mice. In addition, liver function parameters ALT, AST and albumin in plasma were not changed between groups after glucose infusion (Figure S2C).

3.5. The livers of G3PP-LKO mice show enhanced expression of markers of inflammation and macrophage infiltration following chronic hyperglycemia

Increased TG and cholesterol accumulation in the liver is known to trigger inflammation, a characteristic of NAFLD/NASH [30]. Considering

the accumulation of lipids in liver and plasma of glucose infused LKO mice, we measured inflammation markers in the plasma and the expression of the corresponding genes in the liver following glucose infusion. There was no difference in the plasma protein levels of TNF α , IL-6 or CRP between LKO and control mice (Figure 4K) indicating no systemic change in inflammation. However, the mRNA levels of the pro-inflammatory cytokines *Tnfa* and *Il-6* were significantly increased in the hyperglycemic LKO mouse livers compared with control livers (Figure 4L), whereas no changes were seen in the expression of other pro-inflammatory cytokines, *Il-1B* and *Mcp-1*, or the anti-inflammatory cytokine *Il-10* (Figure S2D). Moreover, the mRNA levels of pan-macrophage marker *F4/80* and of the M1-macrophage marker *Cd11c* were markedly increased in the LKO livers compared to the control mice (Figure 4M) suggesting elevated macrophage infiltration.

3.6. Liver metabolites profiling in the G3PP-LKO and control mice during chronic hyperglycemia

Targeted metabolomics (Figure 5 and S3) was conducted in order to gain insight into the mechanism by which G3PP deletion in hepatocytes impacts liver metabolism and physiology *in vivo* under hyperglycemic conditions. The levels of the G3PP substrate, Gro3P and its precursor DHAP (Figure 5A-B) were significantly increased in the LKO mouse liver after 55 h glucose infusion. However, no change was seen in the ATP/ADP ratios (Figure 5D) as well as in ATP, ADP, AMP, adenosine, cAMP (Figure 5P), GTP and GMP levels (Figure S3C) in the LKO livers compared to controls. The redox couples NADH/NAD⁺ (Figure 5E), GSH/GSSG (Figure 5G) as well as parameters that reflect the cytosolic redox state, Gro3P/DHAP (Figure 5C) and pyruvate/lactate (Figure 5H), were similar in both LKO and control livers. An increase in acetyl-CoA and malonyl-CoA levels that positively control the Krebs cycle activity, anaplerosis and lipogenesis, and negatively impact fat oxidation, were found to be higher in the LKO group (Figure 5M-N). The NADPH/NADP ratio was reduced in the LKO livers (Figure 5F), which may reflect increased usage of NADPH for lipogenesis. There was also an increase in the content of some Krebs cycle intermediates, succinate and α -ketoglutarate (Figure 5I-J) in LKO livers, reflecting increased anaplerosis, but not others, (iso)citrate, malate and fumarate (Figure 5K-5 L and S3A). Leucine levels were found to be higher in LKO livers, which may be due to the increased glucose metabolism at elevated glucose in LKO livers (Figure 2F-G) causing less usage of alternative fuels, amino acids and fatty acids (Figure 5O). Other metabolites including pyruvate, lactate, the amino acids alanine, glutamine, glutamate and aspartate were unchanged in the LKO liver (Figure S3A-S3B).

4. DISCUSSION

Glucose derived Gro3P via glycolysis is needed for glycerolipid synthesis at large and TG in particular, and also for shuttling electrons from cytosol to mitochondria via the Gro3P shuttle. Thus, regulation of the cytosolic concentration of Gro3P offers a control mechanism with simultaneous three-dimensional effect on glucose, lipid and energy metabolism, as Gro3P is at the nexus of these pathways [19,22]. Excess supply of glucose can drive elevated production of Gro3P intracellularly and this together with increased availability of FFA, can lead to TG synthesis through the lipogenic arm of the GL/FFA cycle [11,12]. Accumulation of fat in the liver leads to insulin resistance and NAFLD, the hepatic component of the metabolic syndrome, that contributes to the development of obesity and T2D [9,31]. Our earlier *in vitro* studies using isolated rat hepatocytes demonstrated that G3PP expression controls Gro3P levels, particularly at high glucose concentrations [18]. Thus, the G3PP expression level in isolated rat

hepatocytes was found to be inversely related to cellular Gro3P levels and TG accumulation, when cells were incubated at elevated (25 mM) glucose [18]. These *in vitro* observations prompted us to ascertain the role of hepatic G3PP *in vivo*, under both normoglycemic and hyperglycemic conditions.

We now show that liver specific deletion of G3PP in normoglycemic mice fed chow diet leads to [1]: elevated plasma TG with only a small increase in liver TG levels and no changes in body weight and food intake [2]; a small elevated liver glucose production *in vivo* upon a glycerol load but not with a pyruvate load [3]; decreased glycerol shunt with reduced glycerol release and increased gluconeogenesis and lactate production from isolated hepatocytes *ex vivo*. As the alterations in the phenotype of the normoglycemic LKO mice were found to be relatively mild, we tested the consequences of hepatic G3PP deletion *in vivo* in mice with induced chronic hyperglycemia by glucose infusion. Under hyperglycemia, however, very significant changes were observed in the LKO mice [1]: increased plasma TG, LDL, VLDL cholesterol and urea levels [2]; increased liver weight, TG, glycogen, total and free cholesterol contents, as well as expression of markers of inflammation and macrophage invasion [3]; TG deposition in the hearts of LKO mice [4]; elevated liver levels of Gro3P, DHAP, acetyl-CoA, malonyl-CoA and some Krebs cycle intermediates and in the NADP/NADPH ratio. Elevated Krebs cycle intermediates reflect increased anaplerosis (the refilling of cycle intermediates) necessary for lipogenesis and the observed increased levels and malonyl-CoA and TG are indicative of increased lipogenesis in the LKO livers.

What is the mechanism for TG accumulation in mouse hepatocytes with G3PP deletion? One obvious possibility is the elevated availability of Gro3P, due to its decreased hydrolysis [18], for esterification by Gro3P-acyltransferases, leading to increased glycerolipid and TG synthesis. In addition, our study also shows that G3PP deletion results in enhanced anaplerosis and malonyl-CoA formation under conditions of excess glucose supply. This is known to reduce fatty acid oxidation and repartition the fatty acyl groups for lipogenesis. Indeed, in our earlier study using ¹⁴C-palmitate as the tracer in rat hepatocytes with G3PP knockdown, we demonstrated elevated flux of palmitate towards lipogenesis and reduced fatty acid oxidation [18]. Altogether results from our earlier RNAi-knockdown of G3PP in rat hepatocytes and from the present hepatocyte specific G3PP KO mice, indicate that lack of G3PP mediated Gro3P removal in hepatocytes leads to TG accumulation due to elevated Gro3P levels, lipogenesis and reduced fat oxidation.

As there is no change in the weights of adipose depots (Figure S1A) in the G3PP-LKO mice, we do not think that the adipose depots are the source of the elevated liver and plasma TG in these mice. In addition, in the glucose infused mice, the elevated VLDL/LDL (Figure 4H), which carry not only cholesterol but also triglycerides in the plasma, identify liver as the main source of the elevated plasma lipids. The increased lactate production is indicative of increased glycolysis and the elevated acetyl-CoA is known to activate anaplerosis via its effect on pyruvate carboxylase and is also the precursor of cholesterol, which is elevated in the LKO livers. In the present study, we made static measurements of the metabolites and not the flux. Even though, flux measurements using mass isotopes (U-¹³C-glucose) are helpful in tracing the rates of carbon flow, they do not alter the interpretations based on the net static measurements. In the present experiments, we do see strong changes in the levels of several metabolites related to G3PP action and glycerol-3-phosphate hydrolysis, and these changes do indicate altered metabolism due to G3PP deletion in this liver KO model of the enzyme. Overall the results demonstrate that hepatic G3PP is particularly efficient *in vivo* at elevated glucose and that its function is to act as a

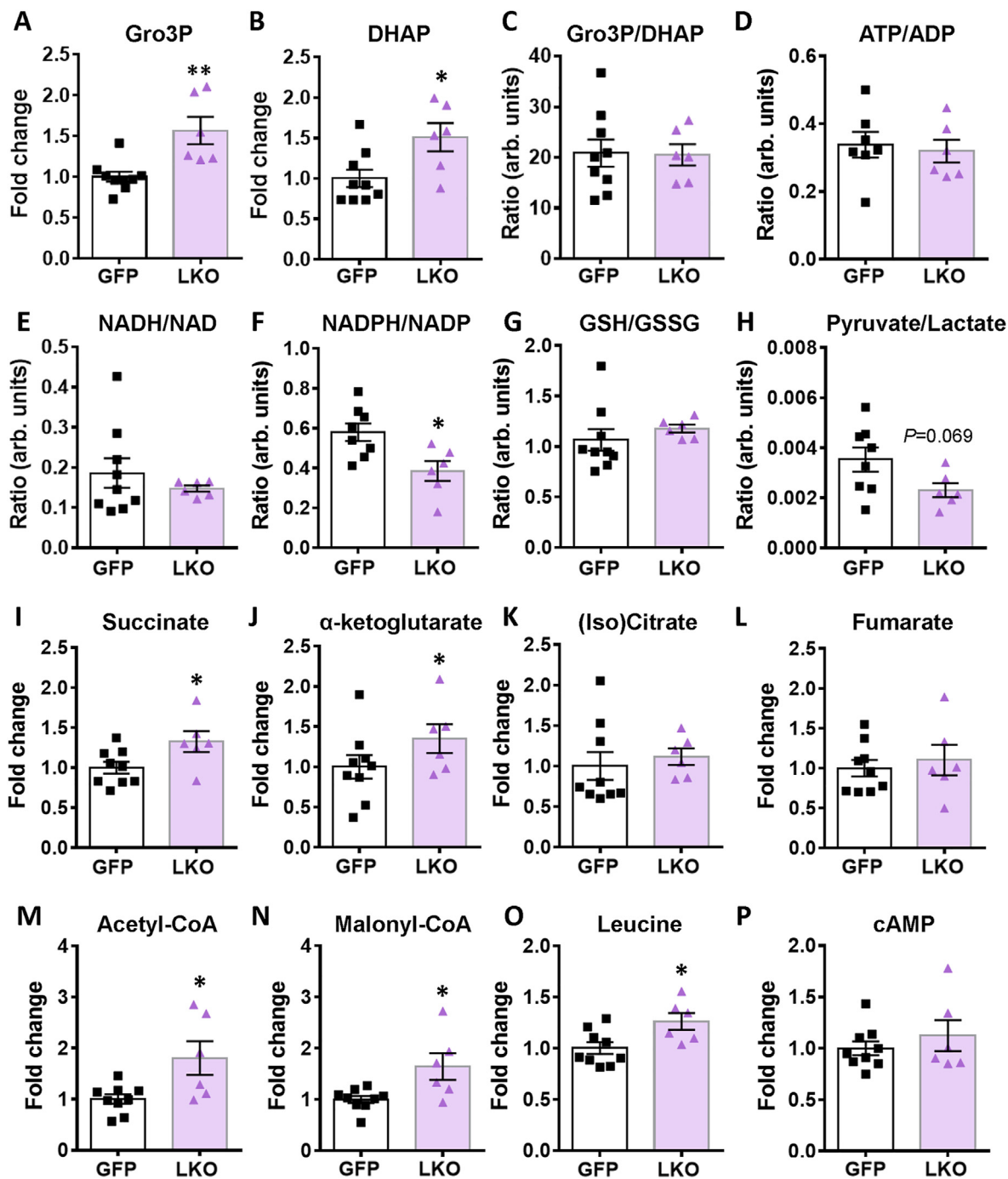


Figure 5: Targeted metabolomic analyses for LKO and control livers following glucose infusion. The indicated metabolites are expressed as fold increase vs GFP-control livers. The ratios of some metabolites and redox couples are shown. (A) Gro3P, (B) DHAP, (C) Gro3P/DHAP, (D) ATP/ADP, (E) NADH/NAD, (F) NADPH/NADP, (G) GSH/GSSG, (H) pyruvate/lactate, (I) succinate, (J) α -ketoglutarate, (K) (iso)citrate, (L) fumarate, (M) acetyl-CoA, (N) malonyl-CoA, (O) leucine and (P) cAMP. Means \pm SEM (GFP-control, n = 9; LKO, n = 6). *p < 0.05, **p < 0.01 vs GFP-control; Student's *t* test.

“glucose excess detoxification machine” or in other words a “glucose excess security valve” in the liver by redirecting the glucose carbons in excess to the glycerol shunt and glycerol release from the hepatocytes. Consistent with this view, in control mice, glycerol level in the urine was elevated by two-fold compared to basal value 6 h after the start of the glucose infusion reaching about 4 mM, and this rise was suppressed in the LKO mice. Noteworthy, glycerol is relatively a less toxic

molecule than glucose, when in excess as high levels of glycerol do not cause any apparent toxicity [32]. Thus upon liver G3PP suppression in mice, there is increased fuel storage in liver in the form of TG, cholesterol and glycogen, as well as enhanced glycolysis and lipogenesis, both *in vivo* and *ex vivo*.

Hepatocyte G3PP deletion accelerated gluconeogenesis starting from glycerol and pyruvate plus lactate, *ex vivo* in isolated LKO hepatocytes,

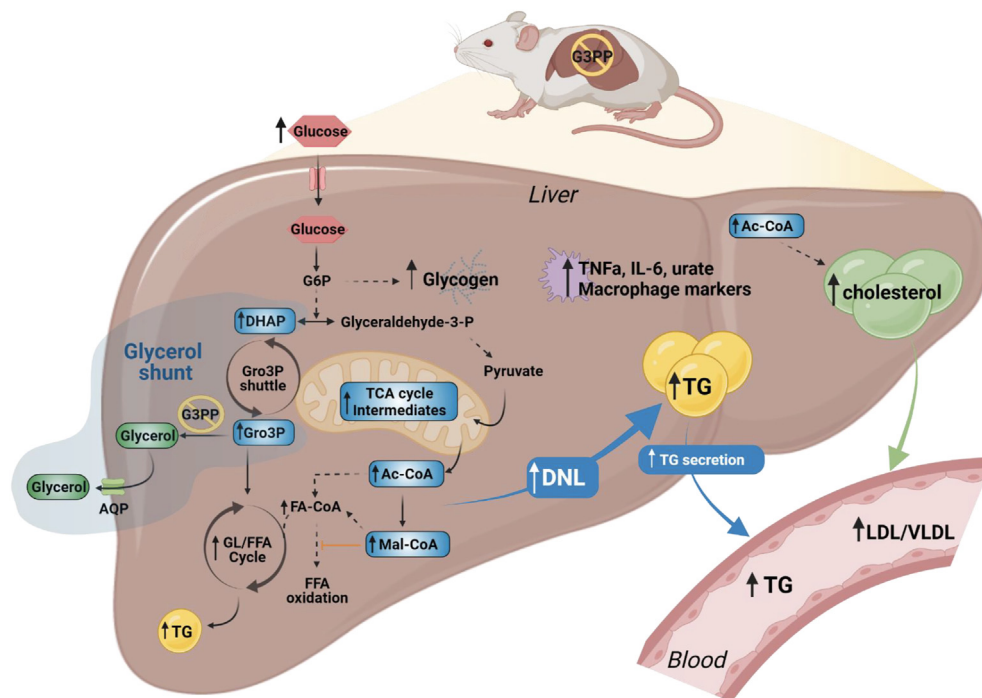


Figure 6: Model depicting the effect of G3PP hepatocyte-specific deletion and suppression of the glycerol shunt on liver metabolism under hyperglycemia. The abbreviations are: Ac-CoA, acetyl-CoA; AQP, aquaglyceroporin; DHAP, dihydroxyacetone phosphate; FA-CoA, fatty acyl-CoA; FFA, free fatty acid; G3PP, glycerol 3-phosphate phosphatase; G6P, glucose 6-phosphate; GL/FFA cycle, glycerolipid/free fatty acid cycle; Glyceraldehyde-3-P, glyceraldehyde-3-phosphate; Gro3P, glycerol 3-phosphate; Mal-CoA, malonyl-CoA; TCA cycle, tricarboxylic acid cycle; TG, triglyceride; LDL, low-density lipoproteins; VLDL, very low-density lipoproteins; DNL, *de novo* lipogenesis.

but surprisingly only with glycerol, *in vivo* and not with pyruvate. It was shown before that glycerol is a better gluconeogenic substrate than lactate or amino acids in mouse liver due to the rapid utilization of glycerol by glycerol kinase [33]. Moreover, it has been shown that lactate is the largest source of gluconeogenic substrate used by kidney [34]. Therefore, in liver G3PP-KO mice, under *in vivo* whole-body conditions, pyruvate is expected to trigger glucose production mostly from kidneys, whereas glycerol is expected to drive gluconeogenesis mainly in hepatocytes.

Deletion of hepatocyte G3PP led to enhanced diversion of Gro3P towards TG synthesis and VLDL packaging and secretion under hyperglycemic conditions. It is possible that the elevated plasma LDL/VLDL facilitated the transport of lipids to tissues like heart, where accumulation of TG was noticed in the LKO mice. In the hyperglycemic LKO mice, the elevated plasma level of urea is possibly related to the enhanced production of acetyl-CoA that is needed for the synthesis of N-acetylglutamate, which drives the first step of urea cycle, catalyzed by carbamoylphosphate synthetase-1 in liver [35]. Increased diversion of glucose carbons towards ribose-5-phosphate and phosphoribosylpyrophosphate synthesis in association with elevated NADPH levels was suggested to lead to elevated formation of uric acid in liver [36], and a combination of glucose, fructose and fatty acids are also known to induce uric acid production in HepG2 cells [37]. Thus, in the hyperglycemic LKO mice, the elevated plasma uric acid may be due to increased diversion of glucose towards pentose pathway and NADPH formation. Furthermore, the higher plasma levels of urea and uric acid seen in the LKO mice, are known biomarkers for hepatic steatosis in patients with NAFLD [38,39].

Elevated succinate observed in the LKO livers is known to regulate inflammation in many tissues including hepatocytes and the hepatic stellate cells, implicated in NAFLD and liver fibrosis [40,41].

Hyperglycemic LKO mouse livers also showed increased levels of leucine, a branched chain amino acid that accumulates as a physiological adaptation to hepatic stress in NAFLD patients [42]. However, the limited duration of hyperglycemic stress did not cause any significant damage to liver as the plasma levels of ALT and AST in the LKO mice were unchanged and similarly many metabolites, including some Krebs cycle intermediates, adenine and guanine nucleotides, many amino acids, cAMP and the redox couples pyruvate/lactate, Gro3P/DHAP, NADH/NAD and GSH/GSSG were unchanged.

Accumulation of hepatic TG and cholesterol is known to promote the activation of macrophages/Kupffer cells, which exacerbate insulin resistance, as well as induce hepatic inflammation and NAFLD progression [30,43,44]. Accordingly, the gene expression of pro-inflammatory cytokines such as TNF α and IL-6, which are known to be released by M1 macrophages and lead to insulin resistance and NAFLD [45], is elevated in LKO livers, together with an increased expression of macrophage markers *Cd11c* (M1 macrophage marker) and *F4/80* (general macrophage marker). These results suggest an enhanced presence of pro-inflammatory oriented macrophages in the livers of hyperglycemic LKO mice, indicating an increased macrophage recruitment and inflammation in the hyperglycemic LKO liver that may in the long term contribute to NAFLD [4,46].

In conclusion, much knowledge has been accumulated concerning the biochemical basis of nutrient excess toxicity in mammalian cells at large and the liver in particular, that include for example ER stress, mitochondrial dysfunction, AMPK inhibition, cholesterol accumulation, the synthesis of some glycerolipids and ROS production. However, much less is known as to how cells can cope with fuel excess and in particular detoxify glucose when elevated. This is more relevant for the hepatocyte and the pancreatic β -cell that express glucokinase, which has high Km for glucose and Vmax, and which rapidly traps influxing

glucose in the cytoplasm in the form of glucose-6-phosphate. Our results, using G3PP LKO mice, identify G3PP and the glycerol shunt as an important glucose excess detoxification pathway in the hepatocyte that when suppressed, under glucotoxic conditions, results in enhanced lipogenesis and accumulation of liver TG, glycogen, and cholesterol, elevated liver inflammation parameters and a rise in plasma TG, uric acid, LDL/VLDL and heart TG (Figure 6). Thus, we propose that the G3PP/glycerol shunt is a novel pathway essential for glucodetoxification and prevention of fat build-up in the liver and that G3PP can be harnessed for metabolic diseases, such as NAFLD/NASH promoted by nutrient excess. Studies in animal models of obesity, diabetes and NAFLD treated with G3PP activators, when they become available, should validate the therapeutic value of G3PP activation.

AUTHOR CONTRIBUTIONS

AAM, MLP, SRMM, and MP designed research; AAM, PP, MLP, RL, IC, YHL, AG and AO conducted experiments; AAM, MLP, SRMM, and MP analyzed data; PP, MLP, EP, YM, RA, FAM and RS critically reviewed and edited the manuscript and AAM, SRMM and MP wrote the paper.

DATA AVAILABILITY

No data was used for the research described in the article.

ACKNOWLEDGMENTS

This study was supported by funds from Canadian Institutes of Health Research (143308, to M.P. and S.R.M.M.), and from Dasman Diabetes Research Institute/Montreal Medical International (to M.P., MSRMM, RA and FA-M). M.P. was recipient up to 2019 of a Canada Research Chair in Diabetes and Metabolism. AA-M is supported by a scholarship from Kuwait University. PP was recipient of postdoctoral fellowships from the Fondation Valifonds, the Montreal Diabetes Research Center, the CRCHUM and Mitacs. We thank the core facilities for Cellular Physiology, Metabolomics and Rodent Phenotyping of the CRCHUM/Montreal Diabetes Research Center. We thank Jennifer Estall and Christopher Rose (University of Montreal, Canada) for helpful advice and discussion. Figures 1A and 6 was created with BioRender.com.

CONFLICT OF INTEREST

The authors have declared that no conflict of interest exists.

APPENDIX A. SUPPLEMENTARY DATA

Supplementary data to this article can be found online at <https://doi.org/10.1016/j.molmet.2022.101609>.

REFERENCES

- Prentki, M., Peyot, M.L., Masiello, P., Madiraju, S.R.M., 2020. Nutrient-induced metabolic stress, adaptation, detoxification, and toxicity in the pancreatic beta-cell. *Diabetes* 69:279–290.
- Nolan, C.J., Prentki, M., 2019. Insulin resistance and insulin hypersecretion in the metabolic syndrome and type 2 diabetes: time for a conceptual framework shift. *Diabetes and Vascular Disease Research* 16:118–127.
- Huang, T.D., Behary, J., Zekry, A., 2020. Non-alcoholic fatty liver disease: a review of epidemiology, risk factors, diagnosis and management. *Internal Medicine Journal* 50:1038–1047.
- Kitade, H., Chen, G., Ni, Y., Ota, T., 2017. Nonalcoholic fatty liver disease and insulin resistance: new insights and potential new treatments. *Nutrients* 9.
- Prentki, M., Corkey, B.E., Madiraju, S.R.M., 2020. Lipid-associated metabolic signalling networks in pancreatic beta cell function. *Diabetologia* 63:10–20.
- Day, C.P., James, O.F., 1998. Hepatic steatosis: innocent bystander or guilty party? *Hepatology* 27:1463–1466.
- Esler, W.P., Bence, K.K., 2019. Metabolic targets in nonalcoholic fatty liver disease. *Cellular and Molecular Gastroenterology and Hepatology* 8:247–267.
- Huang, T.D., Behary, J., Zekry, A., 2019. Non-alcoholic fatty liver disease (NAFLD): a review of epidemiology, risk factors, diagnosis and management. *Internal Medicine Journal* 50(9):1038–1047.
- Birkenfeld, A.L., Shulman, G.I., 2014. Nonalcoholic fatty liver disease, hepatic insulin resistance, and type 2 diabetes. *Hepatology* 59:713–723.
- Duseja, A., Chalasani, N., 2013. Epidemiology and risk factors of nonalcoholic fatty liver disease (NAFLD). *Hepatology International* 7(Suppl 2):755–764.
- Prentki, M., Madiraju, S.R., 2008. Glycerolipid metabolism and signaling in health and disease. *Endocrine Reviews* 29:647–676.
- Prentki, M., Madiraju, S.R., 2012. Glycerolipid/free fatty acid cycle and islet beta-cell function in health, obesity and diabetes. *Molecular and Cellular Endocrinology* 353:88–100.
- Prentki, M., Matschinsky, F.M., Madiraju, S.R., 2013. Metabolic signaling in fuel-induced insulin secretion. *Cell Metabolism* 18:162–185.
- Prentki, M., Nolan, C.J., 2006. Islet beta cell failure in type 2 diabetes. *Journal of Clinical Investigation* 116:1802–1812.
- Oberhauser, L., Maechler, P., 2021. Lipid-induced adaptations of the pancreatic beta-cell to glucotoxic conditions sustain insulin secretion. *International Journal of Molecular Sciences* 23.
- Zechner, R., Zimmermann, R., Eichmann, T.O., Kohlwein, S.D., Haemmerle, G., Lass, A., et al., 2012. Fat signals—lipases and lipolysis in lipid metabolism and signaling. *Cell Metabolism* 15:279–291.
- Poursharifi, P., Attane, C., Mugabo, Y., Al-Mass, A., Ghosh, A., Schmitt, C., et al., 2020. Adipose ABHD6 regulates tolerance to cold and thermogenic programs. *JCI Insight* 5.
- Mugabo, Y., Zhao, S., Seifried, A., Gezzar, S., Al-Mass, A., Zhang, D., et al., 2016. Identification of a mammalian glycerol-3-phosphate phosphatase: role in metabolism and signaling in pancreatic beta-cells and hepatocytes. *Proceedings of the National Academy of Sciences of the United States of America* 113:E430–E439.
- Possik, E., Madiraju, S.R.M., Prentki, M., 2017. Glycerol-3-phosphate phosphatase/PGP: role in intermediary metabolism and target for cardiometabolic diseases. *Biochimie* 143:18–28.
- Al-Mass, A., Poursharifi, P., Peyot, M.L., Lussier, R., Levens, E.J., Guida, J., et al., 2022. Glycerol-3-phosphate phosphatase operates a glycerol shunt in pancreatic beta-cells that controls insulin secretion and metabolic stress. *Molecular Metabolism* 101471.
- Possik, E., Schmitt, C., Al-Mass, A., Bai, Y., Cote, L., Morin, J., et al., 2022. Phosphoglycolate phosphatase homologs act as glycerol-3-phosphate phosphatase to control stress and healthspan in *C. elegans*. *Nature Communications* 13:177.
- Possik, E., Al-Mass, A., Peyot, M.L., Ahmad, R., Al-Mulla, F., Madiraju, S.R.M., et al., 2021. New mammalian glycerol-3-phosphate phosphatase: role in beta-cell, liver and adipocyte metabolism. *Frontiers in Endocrinology* 12:706607.
- Segerer, G., Engelmann, D., Kaestner, A., Trotschmuller, M., Kofeler, H., Stigloher, C., et al., 2018. A phosphoglycolate phosphatase/AUM-dependent link between triacylglycerol turnover and epidermal growth factor signaling. *Biochimica et Biophysica Acta (BBA) - Molecular and Cell Biology of Lipids* 1863:584–594.
- Segerer, G., Hadamek, K., Zundler, M., Fekete, A., Seifried, A., Mueller, M.J., et al., 2016. An essential developmental function for murine phosphoglycolate phosphatase in safeguarding cell proliferation. *Scientific Reports* 6:35160.
- Yan, Z., Yan, H., Ou, H., 2012. Human thyroxine binding globulin (TBG) promoter directs efficient and sustaining transgene expression in liver-specific pattern. *Gene* 506:289–294.

- [26] Bekkevold, C.M., Robertson, K.L., Reinhard, M.K., Battles, A.H., Rowland, N.E., 2013. Dehydration parameters and standards for laboratory mice. *The Journal of the American Association for Laboratory Animal Science* 52:233–239.
- [27] Chew, J.L., Chua, K.Y., 2003. Collection of mouse urine for bioassays. *Lab Animal (NY)* 32:48–50.
- [28] Ochoa-Sanchez, R., Oliveira, M.M., Tremblay, M., Petrazzo, G., Pant, A., Bosoi, C.R., et al., 2021. Genetically engineered *E. coli* Nissle attenuates hyperammonemia and prevents memory impairment in bile-duct ligated rats. *Liver International* 41:1020–1032.
- [29] Cassim, S., Raymond, V.A., Lacoste, B., Lapierre, P., Bilodeau, M., 2018. Metabolite profiling identifies a signature of tumorigenicity in hepatocellular carcinoma. *Oncotarget* 9:26868–26883.
- [30] Chen, Y., Varghese, Z., Ruan, X.Z., 2014. The molecular pathogenic role of inflammatory stress in dysregulation of lipid homeostasis and hepatic steatosis. *Genes & Diseases* 1:106–112.
- [31] Bugianesi, E., Moscatiello, S., Ciaravella, M.F., Marchesini, G., 2010. Insulin resistance in nonalcoholic fatty liver disease. *Current Pharmaceutical Design* 16:1941–1951.
- [32] Lin, E.C., 1977. Glycerol utilization and its regulation in mammals. *Annual Review of Biochemistry* 46:765–795.
- [33] Wang, Y., Kwon, H., Su, X., Wondisford, F.E., 2020. Glycerol not lactate is the major net carbon source for gluconeogenesis in mice during both short and prolonged fasting. *Molecular Metabolism* 31:36–44.
- [34] Gerich, J.E., Meyer, C., Woerle, H.J., Stumvoll, M., 2001. Renal gluconeogenesis: its importance in human glucose homeostasis. *Diabetes Care* 24:382–391.
- [35] Shi, D., Allewell, N.M., Tuchman, M., 2015. The N-acetylglutamate synthase family: structures, function and mechanisms. *International Journal of Molecular Sciences* 16:13004–13022.
- [36] Leyva, F., Wingrove, C.S., Godsland, I.F., Stevenson, J.C., 1998. The glycolytic pathway to coronary heart disease: a hypothesis. *Metabolism* 47:657–662.
- [37] Zhao, L., Guo, X., Wang, O., Zhang, H., Wang, Y., Zhou, F., et al., 2016. Fructose and glucose combined with free fatty acids induce metabolic disorders in HepG2 cell: a new model to study the impacts of high-fructose/sucrose and high-fat diets in vitro. *Molecular Nutrition & Food Research* 60:909–921.
- [38] Liu, X., Zhang, H., Liang, J., 2013. Blood urea nitrogen is elevated in patients with non-alcoholic fatty liver disease. *Hepato-Gastroenterology* 60:343–345.
- [39] Oral, A., Sahin, T., Turker, F., Kocak, E., 2019. Relationship between serum uric acid levels and nonalcoholic fatty liver disease in non-obese patients. *Medicina (Kaunas)* 55.
- [40] Cho, E.H., 2018. Succinate as a regulator of hepatic stellate cells in liver fibrosis. *Frontiers in Endocrinology* 9:455.
- [41] Mills, E., O'Neill, L.A., 2014. Succinate: a metabolic signal in inflammation. *Trends in Cell Biology* 24:313–320.
- [42] Lake, A.D., Novak, P., Shipkova, P., Aranibar, N., Robertson, D.G., Reily, M.D., et al., 2015. Branched chain amino acid metabolism profiles in progressive human nonalcoholic fatty liver disease. *Amino Acids* 47:603–615.
- [43] Matsuzawa, N., Takamura, T., Kurita, S., Misu, H., Ota, T., Ando, H., et al., 2007. Lipid-induced oxidative stress causes steatohepatitis in mice fed an atherogenic diet. *Hepatology* 46:1392–1403.
- [44] Arguello, G., Balboa, E., Arrese, M., Zanlungo, S., 2015. Recent insights on the role of cholesterol in non-alcoholic fatty liver disease. *Biochimica et Biophysica Acta* 1852:1765–1778.
- [45] Odegaard, J.I., Ricardo-Gonzalez, R.R., Red Eagle, A., Vats, D., Morel, C.R., Goforth, M.H., et al., 2008. Alternative M2 activation of Kupffer cells by PPARdelta ameliorates obesity-induced insulin resistance. *Cell Metabolism* 7:496–507.
- [46] Itoh, M., Suganami, T., Kato, H., Kanai, S., Shirakawa, I., Sakai, T., et al., 2017. CD11c+ resident macrophages drive hepatocyte death-triggered liver fibrosis in a murine model of nonalcoholic steatohepatitis. *JCI Insight* 2.